《연구논문》 Korean Journal of Optics and Photonics, Volume 24, Number 5, October 2013
DOI: http://dx.doi.org/10.3807/KJOP.2013.24.5.279

Pressure Dependence of Acoustic Properties of Liquid Ethanol by using High-pressure Brillouin Spectroscopy

Jae-Hyeon Ko[1†], Min-Seok Jeong[1], Byoung Wan Lee[1], Jae Hyun Kim[1], Young Ho Ko[2], Kwang Joo Kim[2], Tae Hyun Kim[3], Seiji Kojima[3], and Muhtar Ahart[4]

[1]*Department of Physics, Hallym University, Hallydaehakgil 1, Chuncheon 200-702, Korea*
[2]*4-2-2, Agency for Defense Development, P.O. Box 35, Yuseong, Daejeon 305-600, Korea*
[3]*Institute of Materials Science, University of Tsukuba, Tsukuba, Ibaraki 305-8573, Japan*
[4]*Geophysical Laboratory, Carnegie Institution of Washington, 5251 Broad Branch Road Northwest, Washington DC 20015, USA*

(Received July 9, 2013; Revised manuscript August 27, 2013; Accepted August 27 2013)

Brillouin spectroscopy has been widely used for the investigation of acoustic properties of condensed matters in the hypersonic region. A high-pressure Brillouin spectrometer was set up by combining a diamond anvil cell and a tandem multi-pass Fabry-Perot interferometer. It was successfully applied to liquid ethanol, and the pressure dependence of the sound velocity, the refractive index and other acoustic properties were derived based on the measurements. The detailed optical setup and experimental procedure are described.

Keywords: Brillouin spectroscopy, High-pressure experiment, Diamond anvil cell, Acoustic property, Elastic constant
OCIS codes: (290.5830) Scattering, Brillouin; (300.6330) Spectroscopy, Inelastic scattering including Raman; (300.6250) Spectroscopy, Condensed matter; (120.5820) Scattering measurements

I. INTRODUCTION

Brillouin scattering belongs to the inelastic light scattering phenomena, which are caused by inelastic scattering events between the incident photons and low-energy excitations thermally excited in condensed matters. This interaction changes the energy of incident photons, and the corresponding frequency shift, which is usually in the hypersonic region, can be measured accurately by a Fabry-Perot interferometer.[1] Propagating density fluctuations in fluids and acoustic phonons in solids are representative examples that are investigated by Brillouin spectroscopy. On the other hand, the optic phonons at the center of the first Brillouin zone can be probed by Raman spectroscopy. The sound velocity, the elastic constants, and the acoustic attenuation coefficient can be obtained in the gigahertz (GHz) frequency range. This method can be combined with the ultrasonic technique operating in the megahertz (MHz) range to investigate the acoustic dispersion effect. The Brillouin scattering phenomenon was theoretically predicted by Brillouin in 1922,[2] and was experimentally confirmed by Gross in 1930.[3]

The advent of coherent laser light source made a breakthrough in inelastic light scattering spectroscopies such as Raman and Brillouin spectroscopies.[4] The introduction of the tandem multi-pass Fabry-Perot interferometer made it possible to obtain high-resolution light scattering spectra in a wide frequency range.[5, 6] In addition, elastic properties of small-size samples, the dimensions of which are the order of a few micrometers, or microheterogeneity of condensed matters could be investigated thanks to the development of the micro-Brillouin spectrometer.[7-9] Quantized vibrations of nanomaterials could also be probed by using micro-Brillouin spectroscopy.[10] Moreover, an angular dispersion-type Fabry-Perot interferometer combined with an area detector can be used to monitor real-time changes in the acoustic properties.[11-13] Excellent review articles on Brillouin spectroscopy can be referred to for more details.[14-17]

One of the main areas to which Brillouin spectroscopy has been applied is the physics of phase transitions.[18, 19] Structural phase transitions caused by the change in a certain thermodynamic variable have attracted great attention from fundamental physics and applications as well. Temperature and pressure are the main two thermodynamic variables that are used to control the phase transition. Temperature variation can be easily achieved by an appropriate temperature controller, while pressure variation needs a special design of a high-pressure

†E-mail: hwangko@hallym.ac.kr
Color versions of one or more of the figures in this paper are available online.

cell such as a diamond anvil cell (DAC). High-pressure Brillouin spectroscopy has been a powerful tool in the investigation of equation of state and/or pressured-induced structural phase transitions of condensed matter.[20-29] In addition, the application of a laser heating technique to DAC may give us a chance of controlling both temperature and pressure of the sample.

Recently, Kim *et al*. successfully developed a high-pressure Brillouin spectrometer and applied this technique to some amorphous materials.[30, 31] The purpose of this study is to report the detailed optical configuration of the high-pressure Brillouin spectrometer set up at Hallym University, to describe the concrete experimental procedure in more detail, and to discuss the experimental results of acoustic properties of liquid ethanol under high pressure obtained by using this spectrometer. This paper will be a complementary work to our previous report on the high-pressure Brillouin spectroscopy.[30] The acoustic properties obtained will be compared to previous studies on ethanol.[32, 33]

II. EXPERIMENT

2.1. Diamond Anvil Cell, Sample Loading, and Pressure Measurements

The diamond anvil cell used in this study has a wide, symmetric aperture, the angle of which is 98°. Figure 1 shows the cross-section of the DAC. It consists of one diamond pair, between which a stainless gasket is inserted. The center of the gasket with a thickness of 250 μm is preindented to a thickness of 50~100 μm, and a circular hole

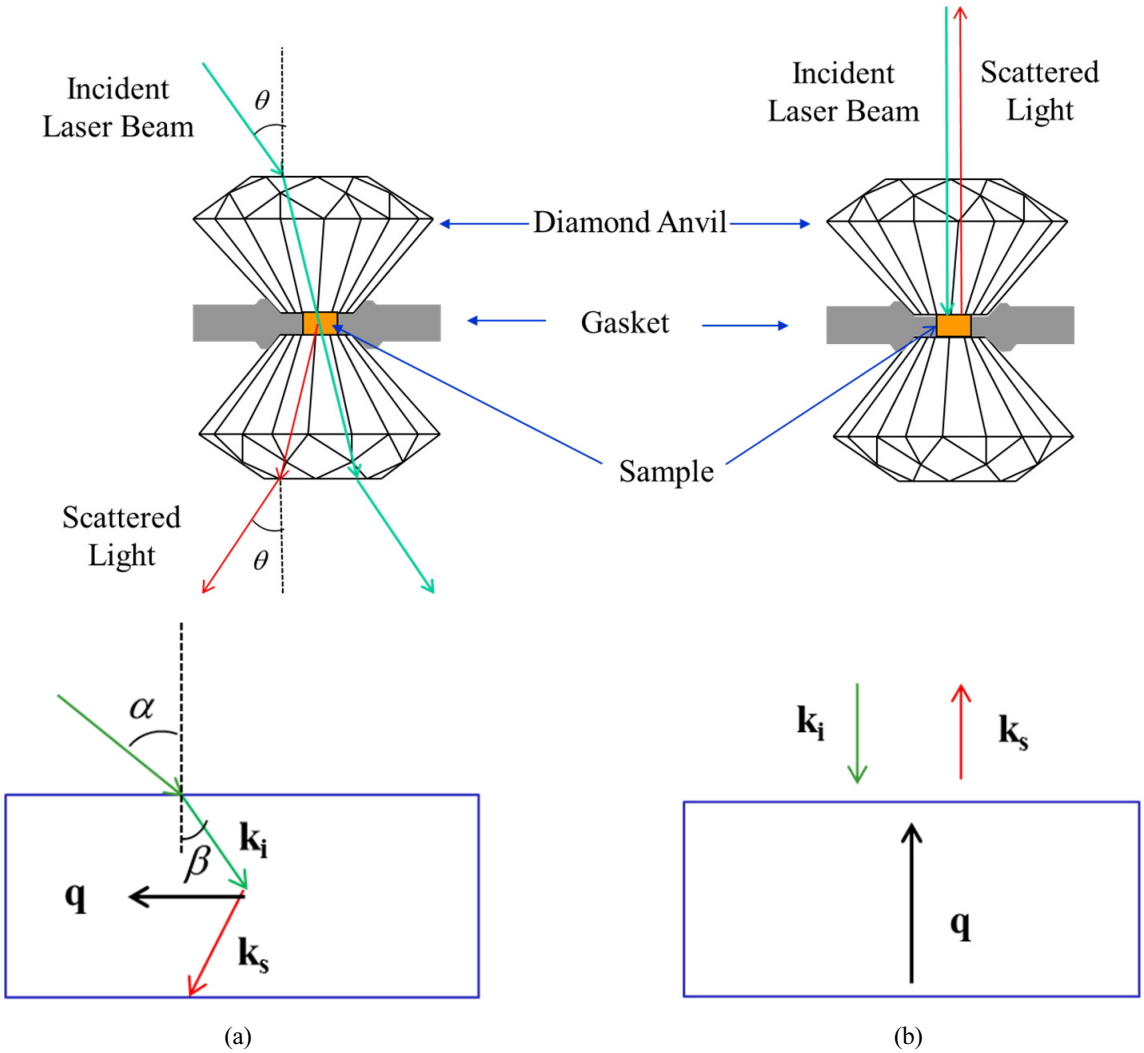

FIG. 1. (a) Forward, symmetric scattering geometry and (b) backscattering geometry. The green and red arrows denote the directions of the laser beam and the scattered light, respectively. $\mathbf{k}_i$, $\mathbf{k}_s$, and $\mathbf{q}$ are the wavevectors of the incident light, the scattered light, and the acoustic phonon, respectively. The lower part of this figure is the extended cross-section of the sample confined in the gasket hole. See the text for more details.

of a diameter of approximately 200 μm is made by using an electric discharge machine (Micro EDM System, Hylozoic Products). The ethanol of high purity (better than 99.9%, Aldrich) was injected into the gasket hole by using a microliter syringe (75N, Hamilton). The four screws of DAC were rotated incrementally to put pressure onto the two diamond anvils, the gasket and the sample in the hole. At each step, the ruby fluorescence spectrum was measured to estimate the pressure as described below.

Two scattering geometries are usually adopted to measure the Brillouin spectrum of the sample in the DAC. In the case of the forward, symmetric scattering geometry shown in Fig. 1(a), the laser beam with a wavelength of λ and the wavevector of $\mathbf{k_i}$ is incident on the flat surface of one of the diamond pair with an incident angle of θ, and is refracted and scattered in the sample. The observation angle for collecting the scattered light with the wavevector of $\mathbf{k_s}$ is usually set to be the same as the incident angle θ. In this case, the refractive index of the sample is not necessary for the calculation of the sound velocity. Let α be the refraction angle in the diamond as shown in the lower left part of Fig. 1, which is the incident angle at the diamond-sample interface. Let β be the refraction angle in the sample. According to the Snell's law, the following relationship is established,

$$\sin\theta = n_d \sin\alpha = n_s \sin\beta \tag{1}$$

where n_d and n_s are the refractive indices of the diamond and the sample, respectively. Therefore, the magnitude of the phonon wavevector, which is defined by $\mathbf{q}=\mathbf{k_s}-\mathbf{k_i}$ according to momentum conservation, is given by the following equation based on the assumption of $k_i \approx k_s \equiv k(=2\pi/\lambda)$.

$$q = 2n_s k \sin\beta = 2k \sin\theta = \frac{4\pi}{\lambda}\sin\theta \tag{2}$$

In the present experiment, the incident angle θ was 30°. The wavevector direction of the scattered light is opposite to that of the incident laser beam at the backscattering geometry, as can be seen from Fig. 1(b). In this case the magnitude of the phonon wavevector becomes maximum and is given by

$$q = 2n_s k = \frac{4\pi n_s}{\lambda}. \tag{3}$$

Pressure measurement was carried out by inserting a few ruby chips in the gasket hole. Figure 2(a) shows the photo of the gasket hole in which ruby chips were immersed in the liquid methanol. Since the ethanol has a high tendency for crystallization at low pressures, we used methanol as the pressure medium for checking the relationship between the ruby fluorescence spectrum and the pressure in a wide range. It is known that methanol can be compressed to high pressures going through the glass transition.[32] The ruby luminescent R lines, excited by the same laser beam as that used for Brillouin scattering, were measured by using a diffraction grating-based spectrometer. Figure 2(b) shows the fluorescence spectrum emitted from the ruby chips at several pressure

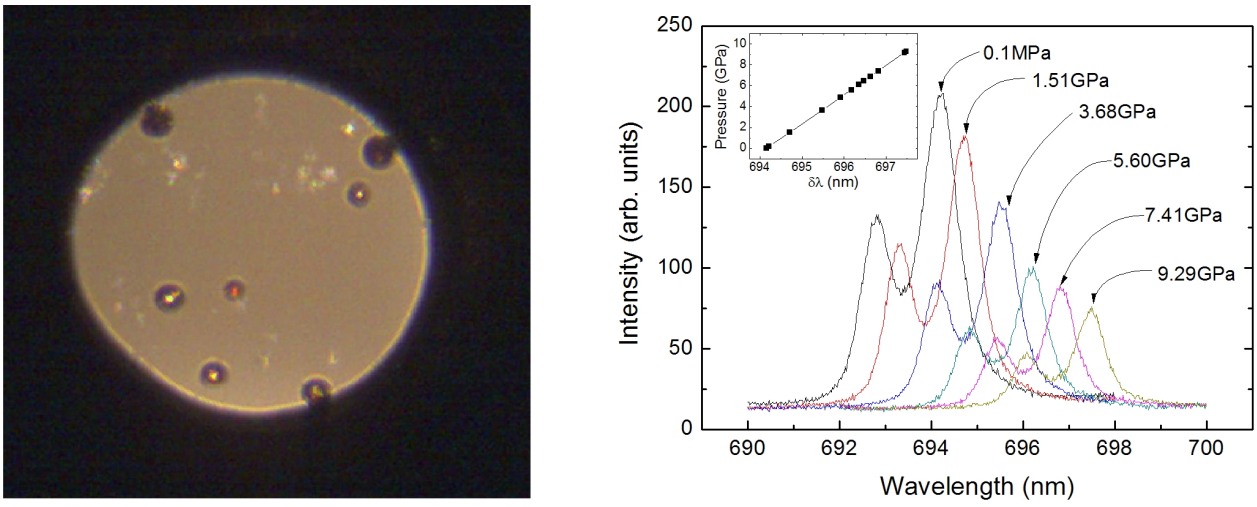

(a) (b)

FIG. 2. (a) A photo of the gasket hole in DAC where a few ruby chips can be seen in ethanol. Small spheres are ruby chips immersed in methanol for pressure measurements. (b) The ruby fluorescence spectra at a few pressure values. The inset shows the dependence of the pressure on the wavelength shift of the R_1 line.

values up to 9.3 GPa. All spectra exhibit two separate peaks called R_1 and R_2 lines with decreasing wavelength. Among the two emitting peaks, the R_1 line was found to shift with pressure P according to the following equation;[34]

$$P = \frac{1904}{B}\left[\left(1+\frac{\delta\lambda}{694.24}\right)^{B}-1\right] \quad (4)$$

where P is given in GPa, $\delta\lambda$ is the wavelength shift of the R_1 line in nm, and B is 7.665 for quasi-hydrostatic conditions. The fluorescence spectrum was fitted by using two Voigt functions, and the center wavelength of the R_1 line was obtained. The pressure was obtained by using Eq. (4). The inset shows that $\delta\lambda$ is approximately linearly proportional to the pressure when the wavelength shift $\delta\lambda$ is small.

2.2. Optical Setup for High-Pressure Brillouin Scattering

Figure 3 shows a schematic diagram of the optical setup used for the present study. A conventional tandem six-pass Fabry-Perot interferometer (TFP-1, JRS Co.) was used for the measurement of scattered light. This interferometer is suitable for high-pressure Brillouin spectroscopy because of the high contrast which is usually the order of 10^{12}. A diode-pumped solid-state laser (Excelsior 532-300, SpectraPhysics) operating at a wavelength (λ) of 532 nm was used as the excitation source. A conventional photon-counting system combined with a multichannel analyser was used to detect and average the signal. Each Brillouin spectrum was obtained for 1024 channels after a few hundred repetitions of accumulation with a gate time of 500 ms for one channel. A micro-Brillouin spectrometer was used for the backscattering experiment, where a modified microscope (BX-41, Olympus) was adopted.[35] A backscattering experiment along with either the DAC or compact temperature chambers (THMS 600 or TS1500, Linkam) can be carried out. The forward, symmetric scattering experiment can be done on the rotation stage on which the DAC can be installed vertically. A compact temperature chamber (FTIR600, Linkam) can also be used on this stage for temperature variation during the experiment. The two scattering geometries described in Fig. 1 can be easily switched by using the translational stage located in front of the entrance pinhole of TFP-1. Another advantage of the present setup is that it can be used for the pressure measurement by using the same microscope and the excitation source. One difference of this optical setup from our previous one[30] is that a right-angle scattering experiment can be carried out at the furnace location in Fig. 3 without

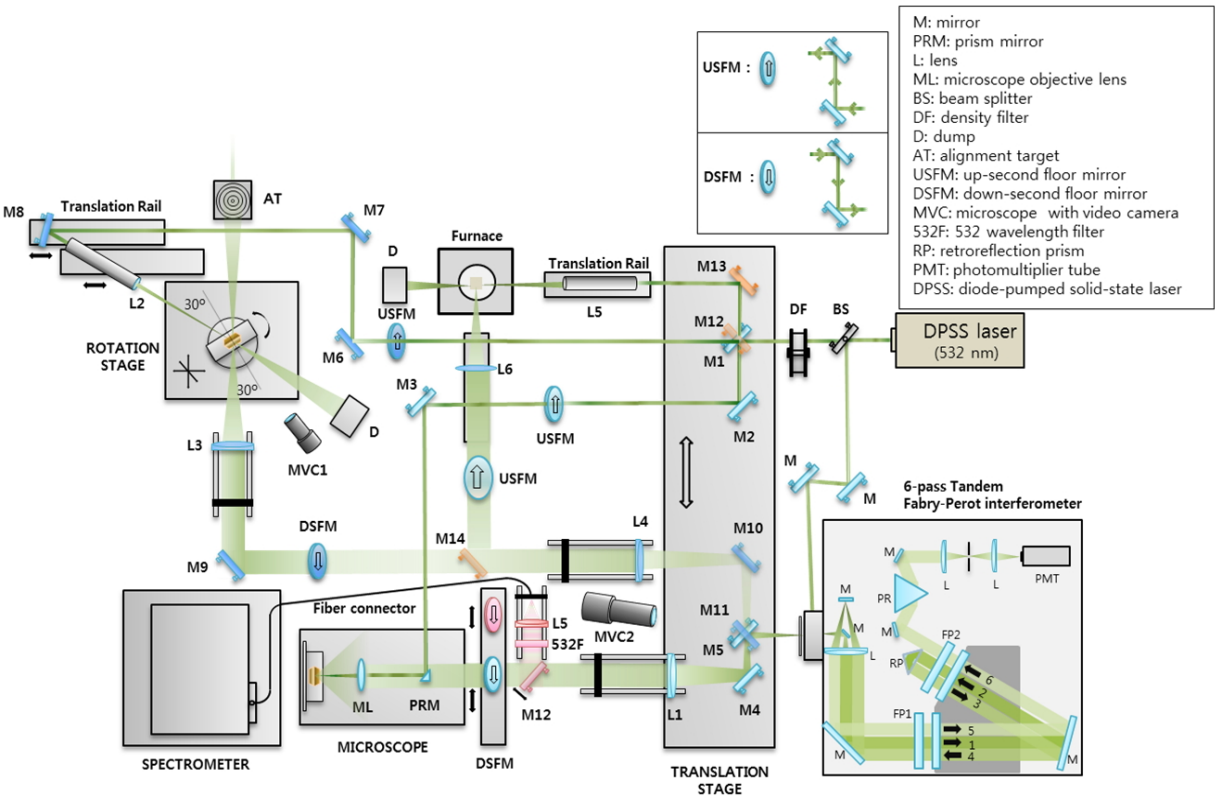

FIG. 3. A schematic diagram of the optical setup for high-pressure Brillouin spectroscopy.

TABLE 1. The list of equipment which can be combined with the Brillouin spectrometer to control either temperature or pressure in a certain range. The possible scattering geometries attainable by each piece of equipment are also included

Thermodynamic variable	Equipment	Measurement range	Scattering geometries
Pressure	Diamond Anvil Cell (symmetric, wide-aperture type)	0.1 MPa~50 GPa	Backward[a] (Micro-Brillouin) Forward, symmetric[b]
Temperature	THMS 600 (Linkam)	-196~600℃	Backward (Micro-Brillouin)
	TS1500 (Linkam)	25~1500℃	
	FTIR 600 (Linkam)	-196~600℃	Backward, Forward, symmetric
	HC-4 MKI (APD cryogenics)	10~300K	Backward, Forward, symmetric Right-angle[c]
	Homemade furnace	25~900℃	

[a]backward scattering geometry as shown in Fig.1(b)
[b]forward, symmetric scattering geometry as shown in Fig.1(a)
[c]right-angle scattering geometry with a scattering angle of 90°

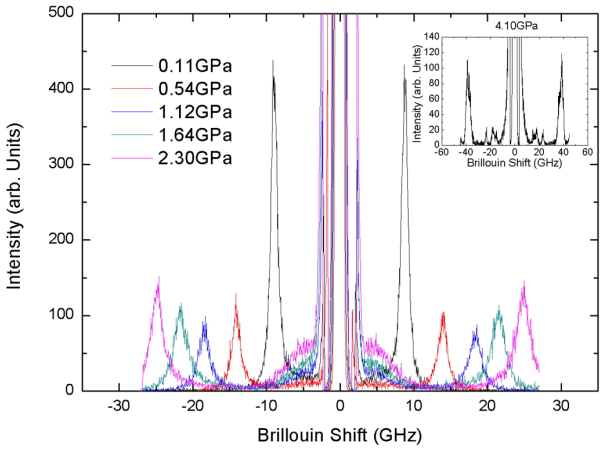

FIG. 4. Brillouin spectra of ethanol at a few pressure values. The inset shows the Brillouin spectrum measured at 4.1 GPa.

changing the remaining setup. A furnace and a He-recycled cryogenic system can be used to change the temperature above and below the room temperature, respectively. The available equipment, which can be combined with the Brillouin spectrometer shown in Fig.3 for controlling either pressure or temperature, is listed in Table 1.

III. RESULT AND DISCUSSION

Figure 4 shows the Brillouin spectrum of ethanol at several pressure values. Each Brillouin spectrum consists of one Brillouin doublet corresponding to the longitudinal acoustic (LA) mode in addition to the unshifted elastic scattering line. The density fluctuation spectrum I_{pp} of an isotropic material with a refractive index n as a function of the angular frequency ω is given by the following equation via a frequency-dependent complex longitudinal modulus $M^*(\omega) = M'(\omega) - M''(\omega)$,[17, 36]

$$I_{\rho\rho} = \frac{I_0}{\omega}\frac{M''(\omega)+\omega\eta_L}{\left[\omega^2\rho/q^2 - M'(\omega)\right]^2 + \left[M''(\omega)+\omega\eta_L\right]^2} \quad (5)$$

where I_0 is a proportionality constant, and η_L is related to the constant, instantaneous damping factor γ_0 via $\eta_L = \rho\gamma_0/q^2$. ρ and $q(=4\pi n\sin\theta/\lambda)$ are the density and the scattering wavevector, respectively. $I_{\rho\rho}$ can be approximated by the response function of a damped harmonic oscillator (DHO) if the acoustic damping is narrower than the dispersion regions, thus $M'(\omega)$ and $M''(\omega)$ can be considered to be constant.[17] The measured spectrum was fitted by using a response function of the DHO for the LA mode. The Brillouin frequency shift (ν_B) and the full-width at half-maximum (FWHM, Γ_B) were obtained as a function of pressure from the curve-fitting procedure. The inset of Fig. 4 shows the Brillouin spectrum of ethanol at 4.1 GPa, which exhibits the asymmetric doublet of the LA mode in addition to at least two doublets corresponding to the transverse acoustic modes. This shows that ethanol is already crystallized at this pressure value. Therefore, the analysis of the acoustic properties of liquid ethanol was limited at and below 2.3 GPa.

Figure 5(a) shows the pressure dependence of ν_B obtained from the backscattering and the forward, symmetric scattering geometries along with the values reported by Ahart *et al.*[33] The two data sets obtained from the backscattering geometry exhibit very similar pressure dependences for the Brillouin shift. Γ_B shown in Fig. 5(b) also shows an increasing behaviour with pressure and seems to reach a maximum at around 1.5~2.0 GPa. This trend is similar to that in the previous report[33] although the absolute value shows some systematic difference. Ahart *et al.* reported that Γ_B shows maximum at approximately 1.5 GPa in both ethanol and methanol.[33] The formation of the hypersonic damping maximum indicates the

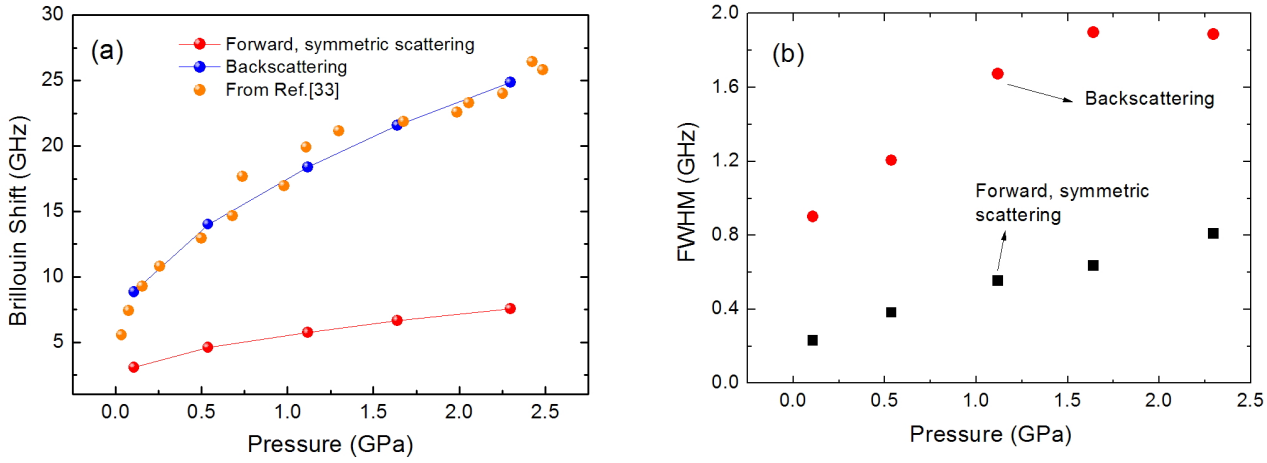

FIG. 5. Pressure dependence of (a) the Brillouin shift and (b) the FWHM of ethanol obtained from the two scattering geometries. The data from Ref.[33] were also shown for comparison.

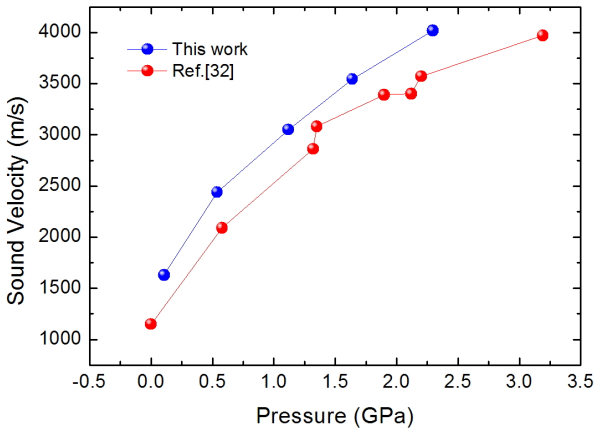

FIG. 6. Pressure dependence of the sound velocity of ethanol obtained from the two scattering geometries. The data from Ref.[32] were also shown for comparison.

proximity of the period of the LA waves to the structural relaxation time in ethanol undergoing the pressured-induced freezing process. That is, the pressure-induced glass transition, which usually makes the coupling between the density fluctuations and the structural relaxation process stronger, is the main origin of the increasing hypersonic damping shown in Fig. 5(b). It is interesting to note that the pressure-induced glass transition is accompanied by substantial growth of the so-called Mountain peak centered at zero frequency, as can be seen from Fig. 5(a). This is additional evidence of the increasing effect of the structural relaxation process on the density fluctuations spectrum in the hypersonic region. Regarding the difference in Γ_B between the backscattering and the forward, symmetric scattering geometry shown in Fig. 5(b), it should be noted that the FWHM of the Brillouin doublet is proportional to q^2/v_B. Since the probed phonon wavevector becomes maximum at the backscattering geometry, it is natural that the Γ_B obtained from the backscattering geometry is much larger than that from the forward, symmetric scattering geometry.

The rapid increase in v_B is associated with the increase in the sound velocity. The sound velocity V can be calculated by combining Eq. (2) or Eq. (3) and $2\pi v_B = qV$ as follows.[37, 38]

$$V = \frac{\lambda v_B}{2n_s} \quad \text{(backscattering)} \tag{6}$$

$$V = \frac{\lambda v_B}{2\sin\theta} \quad \text{(forward, symmetric scattering)} \tag{7}$$

Since there is no information of the pressure dependence of the refractive index, Eq. (7) with θ=30° should be used to calculate the sound velocity in ethanol. The obtained sound velocity is shown in Fig. 6 as a function of pressure. The measurement error for the scattering angle (2θ), which is approximately 1°, induces the uncertainty in the sound velocity of 20~40 m/s. The sound velocity increases from 1630 m/s at 0.1 GPa to 4020 m/s at 2.3 GPa. Previously-reported data obtained by laser-induced phonon spectroscopy[32] were also shown for comparison. Both data sets show similar pressure dependences but exhibit a systematic difference of approximately 100~300 m/s over the investigated pressure range. One possible origin of this difference may be the acoustic dispersion effect, because different length (and frequency) scales were probed in this study and the work of Ref.[32] According to previous studies on ethanol,[36] ethanol exhibits several relaxation processes during the vitrification induced by quenching. The temperature dependence of the

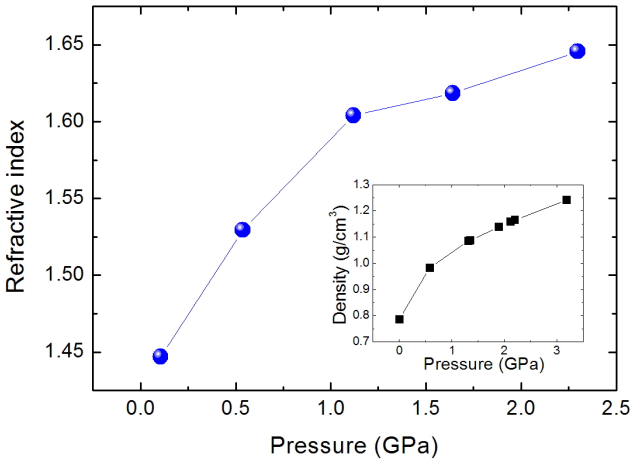

FIG. 7. Pressure dependence of the refractive index of ethanol. The inset shows the pressure dependence of density taken from Ref.[32]

relaxation times of these processes may have substantial effect on the acoustic properties of ethanol depending on the degree of the proximity of the relaxation frequencies and the acoustic frequency. That is, depending on the change of the relaxation time of the relevant process with respect to the inverse of the acoustic frequency, the obtained sound velocity may be either a high-frequency or a low-frequency limiting value resulting in acoustic dispersion. This indicates that the frequency-dependent complex longitudinal modulus $M^*(\omega)$ should reflect the temperature- or pressure-dependent relaxation processes in order to carry out quantitative analysis for the observed acoustic properties, which could become possible in the temperature window.[36] However, there has been no systematic report on the pressure dependence of relaxation processes inherent in ethanol, which makes it difficult to compare the present result with previous study[32] quantitatively.

One more property we can derive from this study is the pressure dependence of the refractive index of ethanol. The combination of Eq. (6) and (7) results in the following equation,[37, 38]

$$n_s = \frac{\nu_B(180^\circ)\sin\theta}{\nu_B(2\theta)} \tag{8}$$

where ν_B (180°) and ν_B (2θ) are the Brillouin shift obtained from the backscattering and the forward, symmetric scattering geometry with a scattering angle of 2θ, respectively. Figure 7 shows the pressure dependence of the refractive index of ethanol. It exhibits a monotonic increase reflecting the increase in the density, because the refractive index is directly related to the density and the molecular polarizability via the Lorentz-Lorenz equation.[26] Since the polarizability is approximately independent of pressure in many liquids, the equation of state shows pressure and temperature behaviors similar to the refractive index.[37, 38] As the Fig. 7 shows, both properties show a rapid increase at low pressures below~1 GPa and exhibits a relatively mild increase at high pressures.

IV. CONCLUSION

A high-pressure Brillouin spectrometer was developed for the investigation of acoustic properties of condensed matters. Brillouin scattering experiments at backscattering, right-angle scattering and forward, symmetric scattering geometries, in addition to *in situ* pressure measurement, could be carried out on the optical bench without any substantial change in the optical configuration. The pressure dependence of the Brillouin scattering spectrum of liquid ethanol was measured from ambient condition up to 4.1 GPa. The Brillouin shift showed monotonic increase while the half width exhibited a broad maximum in 1.5~2 GPa, indicating significant coupling between the density fluctuations and the structural relaxation process. The pressure dependence of the sound velocity and the refractive index of ethanol could be obtained. The Brillouin spectrum at the highest pressure of 4.1 GPa showed split LA and TA modes, which was a signal of crystallization of ethanol.

ACKNOWLEDGMENT

This work was supported by the Defense Research Laboratory Program of the Defense Acquisition Program Administration and the Agency for Defense Development of Republic of Korea and by the Basic Science Research Program through the National Research Foundation of Korea (NRF) funded by the Ministry of Education, Science and Technology (2013 R1A1A2006582).

References

1. W. Hayes and R. Loudon, *Scattering of Light by Crystals* (Wiley, New York, USA, 1978), Chapter 7.
2. L. Brillouin, “Diffusion de la lumière et des rayons X par un corps transparent homogène: Influence de l’agitation thermique,” Ann. Physique **17**, 88-122 (1922).
3. E. Gross, “Change of wavelength of light due to elastic heat waves at scattering in liquids,” Nature **126**, 201-202 (1930).
4. H. Z. Cummins and R. W. Gammon, “Rayleigh and Brillouin scattering in liquids-Landau-Placzek ratio,” J. Chem. Phys. **44**, 2785-2796 (1966).
5. J. R. Sandercock, “Some recent developments in Brillouin scattering,” RCA Rev. **36**, 89-107 (1975).

6. J. R. Sandercock, *Light Scattering in Solids III*, M. Cardona and G. Güntherodt eds. (Springer, Berlin, 1982), p. 173.
7. Y. Takagi and K. Kurihara, "Application of a microscope to Brillouin scattering spectroscopy," Rev. Sci. Instrum. **63**, 5552-5555 (1992).
8. M. Ahart, T. Yagi, and Y. Takagi, "Microscopic Brillouin scattering study in TeO_2-pressure dependence of acoustic modes," Jpn. J. Appl. Phys. **35**, 2882-2888 (1996).
9. F. M. Jiang and S. Kojima, "Microheterogeneity and relaxation in $0.65Pb(Mg_{1/3}Nb_{2/3})O_3$-$0.35PbTiO_3$ relaxor single crystals," Appl. Phys. Lett. **77**, 1271-1273 (2000).
10. Y. Li, H. S. Lim, S. C. Ng, Z. K. Wang, M. H. Kuok, E. Vekris, V. Kitaev, F. C. Peiris, and G. A. Ozin, "Micro-Brillouin scattering from a single isolated nanosphere," Appl. Phys. Lett. **88**, 023112 (2006).
11. S. Itoh, T. Yamana, and S. Kojima, "Quick measurement of Brillouin spectra of glass-forming material Trimethylene Glycol by angular dispersion-type Fabry-Perot interferometer system," Jpn. J. Appl. Phys. **35**, 2879-2881 (1996).
12. J.-H. Ko and S. Kojima, "Nonscanning Brillouin spectroscopy applied to solid materials," Rev. Sci. Instrum. **73**, 4390-4392 (2002).
13. J.-H. Ko and S. Kojima, "Angular dispersion-type nonscanning Fabry-Perot interferometer applied to ethanol-water mixture," J. Opt. Soc. Korea **13**, 261-266 (2009).
14. H. Z. Cummins and P. E. Schoen, *Laser Handbook*, F. T. Arecchi and E. O. Schulz-Dubois eds. (North-Holland, Amsterdam, 1972), pp. 1029-1075.
15. R. Vacher and L. Boyer, "Brillouin scattering: A tool for the measurement of elastic and photoelastic constants," Phys. Rev. B **6**, 639-673 (1972).
16. S. Kojima, "Gigahertz acoustic spectroscopy by micro-Brillouin scattering," Jpn. J. Appl. Phys. **49**, 07HA01 (2010).
17. L. Comez, C. Masciovecchio, G. Monaco, and D. Fioretto, "Progress in liquid and glass physics by Brillouin scattering spectroscopy," Solid State Phys. **63**, 1-77 (2012).
18. H. Z. Cummins, "Brillouin scattering spectroscopy of ferroelectric and ferroelastic phase transitions," Phil. Trans. R. Soc. Lond. A **293**, 393-405 (1979).
19. H. Z. Cummins and A. P. Levanyuk, *Light Scattering Near Phase Transitions* (Elsevier Science, Oxford, 1983).
20. C. H. Whitfield, E. M. Brody, and W. A. Bassett, "Elastic moduli of NaCl by Brillouin scattering at high pressure in a diamond anvil cell," Rev. Sci. Instrum. **47**, 942-947 (1976).
21. H. Shimizu, E. M. Brody, H. K. Mao, and P. M. Bell, "Brillouin measurements of solid *n*-H_2 and *n*-D_2 to 200 kbar at room temperature," Phys. Rev. Lett. **47**, 128-131 (1981).
22. M. Grimsditch, R. Bhadra, and Y. Meng, "Brillouin scattering from amorphous materials at high pressure," Phys. Rev. B **38**, 7836-7838 (1988).
23. C.-S. Zha, T. S. Duffy, H.-K. Mao, and R. J. Hemley, "Elasticity of hydrogen to 24 GPa from single-crystal Brillouin scattering and synchrotron x-ray diffraction," Phys. Rev. B **48**, 9246-9255 (1993).
24. T. S. Duffy, W. L. Vos, C.-S. Zha, R. J. Hemley, and H.-K. Mao, "Sound velocities in dense hydrogen and the interior of Jupiter," Science **263**, 1590-1593 (1994).
25. C.-S. Zha, R. J. Hemley, H.-K. Mao, T. S. Duffy, and C. Meade, "Acoustic velocities and refractive index of SiO_2 glass to 57.5 GPa by Brillouin scattering," Phys. Rev. B **50**, 13105-13112 (1994).
26. A. Polian, "Brillouin scattering at high pressure: An overview," J. Raman Spectrosc. **34**, 633-637 (2003).
27. M. Ahart, J. L. Yarger, K. M. Lantzky, S. Nakano, H.-K. Mao, and R. J. Hemley, "High-pressure Brillouin scattering of amorphous BeH_2," J. Chem. Phys. **124**, 014502 (2006).
28. L. L. Stevens, E. B. Orler, D. M. Dattelbaum, M. Ahart, and R. J. Hemley, "Brillouin-scattering determination of the acoustic properties and their pressure dependence for three polymeric elastomers," J. Chem. Phys. **127**, 104906 (2007).
29. A. S. Benjamin, M. Ahart, S. A. Gramsch, L. L. Stevens, E. B. Orler, D. M. Dattelbaum, and R. J. Hemley, "Acoustic properties of Kel F-800 copolymer up to 85 GPa," J. Chem. Phys. **137**, 014514 (2012).
30. J. H. Kim, J.-Y. Choi, M.-S. Jeong, J.-H. Ko, M. Ahart, Y. H. Ko, and K. J. Kim, "Development of a high-pressure Brillouin spectrometer and its application to an ethylene-vinyl acetate copolymer," J. Korean Phys. Soc. **60**, 1419-1423 (2012).
31. M.-S. Jeong, J. H. Kim, J.-H. Ko, Y. H. Ko, and K. J. Kim, "Pressure dependence of acoustic behaviors and refractive index of amorphous Kel F-800 copolymer studied by Brillouin spectroscopy," Curr. Appl. Phys. **13**, 1774-1777 (2013).
32. J. M. Brown, L. J. Slutsky, K. A. Nelson, and L.-T. Cheng, "Velocity of sound and equations of state for methanol and ethanol in a diamond-anvil cell," Science **241**, 65-67 (1988).
33. M. Ahart, F. Jiang, and S. Kojima, "Brillouin scattering of pressure-induced glass transition in ethanol and methanol," Jpn. J. Appl. Phys. **37**, 1052-1053 (1998).
34. M. I. Eremets, *High Pressure Experimental Methods* (Oxford University Press, Oxford, 1996), Chapter 12.
35. T. H. Kim, J.-H. Ko, E. M. Kwon, and J.-G. Jun, "Micro-Brillouin spectroscopy applied to the glass transition of anti-inflammatory egonol," J. Opt. Soc. Korea **14**, 403-408 (2010).
36. J.-H. Ko and S. Kojima, "Brillouin scattering study on glass-forming ethanol," J. Non-cryst. Solids **307-310**, 154-160 (2002) and references therein.
37. R. Jia, F. Li, M. Li, Q. Cui, Z. He, L. Wang, Q. Zhou, T. Cui, G. Zou, Y. Bi, S. Hong, and F. Jing, "Brillouin scattering studies of liquid argon at high temperatures and high pressures," J. Chem. Phys. **129**, 154503 (2008).
38. F. Li, M. Li, Q. Cui, T. Cui. Z. He, Q. Zhou, and G. Zou, "The velocity, refractive index, and equation of state of liquid ammonia at high temperatures and high pressures," J. Chem. Phys. **131**, 134502 (2009).